

Bioadhesive Hydrogel-Coupled and Miniaturized Ultrasound Transducer System for Long-Term, Wearable Neuromodulation

AUTHOR INFORMATION

Kai Wing Kevin Tang^{1,†}, Jinmo Jeong^{1,†}, Ju-Chun Hsieh^{1,†}, Mengmeng Yao¹, Hong Ding¹, Wenliang Wang¹, Xiangping Liu¹, Ilya Pyatnitskiy¹, Weilong He¹, William D. Moscoso-Barrera¹, Anakaren Romero Lozano¹, Brinkley Artman¹, Heeyong Huh², Preston S. Wilson³, Huiliang Wang^{1*}

AFFILIATION

¹*Department of Biomedical Engineering, Cockrell School of Engineering, The University of Texas at Austin, Austin, Texas 78712, United States.*

²*Department of Aerospace Engineering and Engineering Mechanics, Cockrell School of Engineering, The University of Texas at Austin, Austin, Texas 78712, United States.*

³*Walker Department of Mechanical Engineering, Cockrell School of Engineering, The University of Texas at Austin, Austin, Texas 78712, United States.*

[†]These authors contributed equally to this work.

*Corresponding author

Corresponding Author: Dr. Huiliang (Evan) Wang

Department of Biomedical Engineering, Cockrell School of Engineering, The University of Texas at Austin, Austin, Texas 787112, United States

E-mail: evanwang@utexas.edu

Keywords: (ultrasound, neuromodulation, hydrogel, wearable devices)

28 **Abstract**

29 Transcranial focused ultrasound has become a promising non-invasive approach for
30 neuromodulation applications, particularly for neurodegenerative diseases and psychiatric
31 illnesses. However, its implementation in wearable neuromodulation has thus far been limited due
32 to the devices' large size, which needs external supporting systems for the neuromodulation
33 process. Furthermore, the need for ultrasound gel for acoustic coupling between the device and
34 skin limits the viability for long-term use, due to its inherent susceptibility to dehydration and lack
35 of adhesiveness to form a stable interface. Here, we report a wearable miniaturized ultrasound
36 device with size comparable to standard EEG/ECG electrodes integrated with bioadhesive
37 hydrogel to achieve efficient acoustic intensity upon ultrasound stimulation for long-term,
38 wearable primary somatosensory cortical stimulation. Specifically, air-cavity Fresnel lens
39 (ACFAL) based self-focusing acoustic transducer (SFAT) was fabricated using a lithography-free
40 microfabrication process. Our transducer was able to achieve an acoustic intensity of up to 30.7
41 W/cm² (1.92 MPa) in free-field with a focal depth of 10 mm. Bioadhesive hydrogel was developed
42 to address the need for long-term stability of acoustic couplant for ultrasound application. The
43 hydrogel demonstrated less than 13% attenuation in acoustic intensity and stable adhesion force
44 of 0.961 N/cm over 35 days. Leveraging our bioadhesive hydrogel-integrated wearable ultrasound
45 transducer, we were able to suppress somatosensory evoked potentials elicited by median nerve
46 stimulation via functional electrical stimulation over 28 days, demonstrating the efficacy of our
47 transducer for long-term, wearable neuromodulation in the brain.

48 **Introduction**

49 The increase in brain diseases amongst the general population has motivated significant
50 research in therapeutic treatment approaches. With 1 million people in the US diagnosed with
51 Parkinson's disease and a projected increase of 78% annually, the socioeconomic burden on
52 individuals, families, and the healthcare system is significant^{1,2}. Deep brain stimulation (DBS) has
53 been clinically approved in treating Parkinson's disease³⁻⁷, essential tremor⁸⁻¹², epilepsy¹³⁻¹⁶,
54 dystonia¹⁷⁻¹⁹ and obsessive-compulsive disorder^{4,20}. Despite being a very effective method, it
55 requires invasive implanted electrodes with complications involving hematoma, lead fractures, and
56 glial response rendering electrodes ineffective^{21,22}. Alternatively, non-invasive brain stimulation
57 devices provide a unique opportunity for novel treatments for a multitude of psychiatric, mental,
58 and neurodegenerative diseases in a substantial number of patients as a non-invasive intervention.
59 Transcranial magnetic stimulation (TMS) are currently effective and clinically approved treatment
60 methods for mental health disorders such as obsessive-compulsive disorders and depression²³. It
61 has also shown promising improvements in sleep disorders, Parkinson's²⁴, Alzheimer's²⁵ and
62 potentially several other neuropsychiatric disorders²⁶. However, TMS stimulates large brain areas
63 due to its low spatial resolution, making it difficult to achieve the most effective treatment without
64 causing adverse off-targeting effects²⁷⁻³⁰. Since TMS generally requires a 3~6 weeks treatment
65 period and DBS require continuous stimulation upon implantation, there is a strong need for non-
66 invasive and high-spatial resolution neuromodulation approach with long-term wearability^{6,25,31-}
67 ³³.

68 Transcranial focused ultrasound (tFUS) provides an alternative non-invasive strategy for
69 highly precise targeting of subcortical and deep brain stimulation with high spatial-temporal
70 resolution³⁴. It has shown improvement in neurological diseases such as tremor associated with
71 Parkinson's disease^{35,36}, cognitive and memory impairments in Alzheimer's disease³⁷⁻⁴¹,
72 epilepsy⁴²⁻⁴⁴, and chronic mental health disorders⁴⁵. However, the current tFUS systems are
73 typically bulky and are not in wearable format for long-term neuromodulation. To develop an
74 effective wearable ultrasound neuromodulation system requires: 1) miniaturized transducer with
75 effective acoustic intensity and focality for tFUS⁴⁶, 2) stable fixation to the skin during
76 neuromodulation⁴⁷, and 3) acoustic impedance match between the ultrasound transducer and
77 tissue⁴⁸. Currently, the commercial ultrasound gel has been commonly used as a medium to match
78 the acoustic impedance during ultrasound stimulation by eliminating air gaps in promoting the

79 efficiency of ultrasound transmission⁴⁹. Yet, its limitations of non-adhesive properties for
80 ultrasound transducer fixation to the skin and dehydration susceptibility prevents long-term use in
81 continuous neuromodulation treatment of brain disorders over several weeks⁵⁰. Current
82 approaches in developing acoustic hydrogel for wearable ultrasound imaging application has
83 shown to be effective for ultrasound applications, however its efficacy diminishes drastically after
84 72 hours^{51,52}. Therefore, a wearable ultrasound device integrated with an acoustically compatible
85 medium that provides robust device-to-skin adhesion for long-term application is desired.

86 In this work, we developed a strategy to address the current limitations of ultrasound
87 devices to enable long-term cortical neuromodulation. Specifically, we have developed self-
88 focusing acoustic transducers (SFAT) that leverages geometrical patterning of acoustic lens in
89 altering wave propagation to achieve acoustic focusing through the use of air-cavity fresnel
90 acoustic lens (ACFAL), allowing an increase in acoustic intensity of the focal depth limit originally
91 constrained by the geometrical diameter of the transducer (**Fig. 1a-c**)⁵³. In addition, we have
92 designed bioadhesive hydrogel, consisting of 2-acrylamido-2-methyl-1-propanesulfonic acid
93 (AMPS) and glycerol, to have high water absorption and rehydration properties over a month and
94 strong adhesion to the skin (**Fig. 1d**). Through integration of bioadhesive hydrogel to our SFAT
95 transducer, our **Miniaturized and Bioadhesive-coupled Ultrasound Transducer (MiniUITra)**
96 weighs 8.5 grams and can be easily attached to the target skin for an extended period, allowing
97 ease of use for long-term applications (**Fig. 1e-h**). We evaluated the efficacy of MiniUITra in its
98 effectiveness in suppressing somatosensory evoked potential elicited by median nerve stimulation
99 via functional electrical stimulation over 28 days, demonstrating the efficacy of MiniUITra in long-
100 term cortical neuromodulation as a wearable ultrasound device.

101

102 **Results**

103 **Development and characterization of miniaturized ultrasound transducer**

104 Acoustic frequencies used for ultrasound stimulation with ideal transcranial transmission
105 and brain absorption has been reported to be within the 500 kHz to 750 kHz range^{54,55}, where
106 clinical demonstration of using ultrasound stimulation at the 650 kHz frequency in humans has
107 shown effective suppression evoked potential and enhanced sensory functions⁵⁶. Thus, we
108 developed a custom miniaturized 650 kHz ultrasound transducer (similar size to standard EEG
109 electrode leads, OD = 18 mm) with microfabrication techniques to create a self-focusing acoustic

110 transducer (SFAT) using air cavity Fresnel acoustic lens (ACFAL) coupled with a novel highly
111 adhesive and conformable bioadhesive hydrogel for long-term applications. Characterization of
112 acoustic pressure fields emitted from our SFAT-ACFAL was done using a calibrated hydrophone
113 (**Fig. 2a**) on a motorized 3-axis system submerged in a degassed distilled water bath. Comparison
114 of acoustic field distribution with and without the ACFAL formed by PDMS (Pristine PZT/SFAT-
115 ACFAL) showed less scattering and higher focusing on the desired focal point in the transducer
116 with ACFAL (**Fig. 2b**). Recording of acoustic waveforms pulsed and transmitted was performed
117 in free-field and with a macaque skull, where measurements indicate a spatial focality of 3.5 mm
118 axially and 8 mm radially (**Fig. 2c-d**). The focal depth was measured to be at 10 mm, at the
119 expected and designed specification. To determine the acoustic intensity and biosafety of the
120 devices for ultrasound neuromodulation, a calibration curve was performed with our ultrasound
121 system (Image Guided Therapy System) used to drive the SFAT-ACFAL to evaluate the linearity
122 of acoustic intensity and pressure when driving amplitude was increased. The measurements
123 revealed a spatial-peak pulse-average intensity (I_{SPPA}) in the free field to be less than 30.7 W/cm^2
124 (1.92 MPa) (**Fig. 2e**). However, free-field acoustic intensity of 23.9 W/cm^2 has shown to be
125 effective when transmitting through the human skull with a four-fold drop in intensity to 5.9 W/cm^2
126 ⁵⁶. Therefore, all stimulation paradigms performed in healthy volunteers using our device were
127 performed at 23.1 W/cm^2 (1.66 MPa), to necessitate sufficient acoustic intensity threshold in
128 suppression of sensory evoked potentials⁵⁶. The effect of transcranial skull transmission effectively
129 attenuates the amplitude of the acoustic pulse waveform (**Fig. 2f**) and increases the spatial
130 resolution of the focal spot. This is suspected due to the inhomogeneity of skull and tissue
131 interfaced between the boundary conditions resulting in time-reversible wave propagation,
132 commonly used for imaging⁵⁷. The shift in axial peak of the focal spot (**Fig. 2d**) was due to the
133 curvature of the macaque skull and its difficulty in positioning between the hydrophone and device
134 to prevent collision.

135 To ensure thermal biosafety, the device during ultrasound stimulation should not exceed
136 an increase of 2°C ⁵⁸. We then characterized the thermal biosafety of the device by performing the
137 stimulation paradigm used by Legon *et al.*⁵⁶ in comparison with higher duty cycle and pulse
138 duration through the macaque skull and monitoring the temperature of the stimulation site using
139 an infrared camera (**Fig. 2g, Supplementary Fig. 1**). Results indicated that with 10 min of
140 continuous stimulation, the paradigm of $360 \mu\text{s}$ ON and $640 \mu\text{s}$ OFF ⁵⁶ had no thermal increase.

141 Similarly, when the duty cycle was increased to 50% (500 μ s ON and 500 μ s OFF) there was no
142 significant temperature increase. However, when the pulse duration increased to 50 ms ON and 50
143 ms OFF, drastic temperature increase was observed beyond the 5 min mark. This demonstrates the
144 safety regime of the device for human applications. Electrical characterization of the device was
145 performed using an impedance spectrum analyzer to determine the impedance and phase response
146 of SFAT-ACFAL. The impedance was then used to determine harmonic frequencies where
147 impedance is lowest for impedance matching purposes (**Fig. 2h**).

148

149 **Development and characterization of bioadhesive hydrogel**

150 To ensure long-term neuromodulation viability, the need for an acoustic couplant to sustain
151 stable acoustic properties over time is needed to be integrated with the SFAT-ACFAL.
152 Specifically, it should sustain hydration, effectively transmit ultrasound, adhere conformally to the
153 skin with a low modulus to minimize air gaps, and maintain high adhesion force over time^{51,52}.
154 The bioadhesive hydrogel used in this study includes two primary materials: 1) 2-acrylamido-2-
155 methylpropane sulfonic acid (AMPS) and 2) glycerol (**Fig. 1d**). PolyAMPS is an ionic polymer
156 with a hydrophilic sulfonic group resulting in it being inherently negatively charged, which allows
157 for strong ionic interaction with water molecules⁵⁹. Thus, it enables high water absorption rate⁶⁰⁻
158 ⁶², allowing sustained hydrated state through absorption of ambient moisture⁶³. In addition to its
159 high water content and retention, PolyAMPS provides modulus similar to that of biological
160 tissues⁶⁴, and is suitable as a long-term substitute of commercially available ultrasound gel that
161 tends to dehydrate within hours. Furthermore, the addition of glycerol containing hydroxyl groups,
162 which forms hydrogen bonds with water molecules, provides water retention capacity and
163 enhanced adhesion to the skin by offering a hydrating effect on the stratum corneum^{60,65,66}.

164 We characterized the acoustic attenuation rate of our bioadhesive hydrogel at different
165 thickness in comparison to commercial gel. As a result, we observe that the ultrasound power
166 attenuation of the bioadhesive hydrogel is comparable to that of commercial gel at thicknesses of
167 0.5 mm and 1 mm (**Fig. 3a**). With ultrasound as a mechanical acoustic wave, the mismatch in
168 impedance when propagated between mediums with varying acoustic impedances inevitably leads
169 to partial transmission and reflection at the boundary layers. By minimizing the mismatch in
170 impedance, reduction of reflected and maximizing transmitted waves provides higher acoustic
171 intensity deposition to the target site. Therefore, the need for minimizing the impedance mismatch

172 between our device and the skin using our bioadhesive hydrogel is necessary⁵¹. As acoustic speed
173 in a material is directly related to its elastic properties and density, the acoustic impedance could
174 be derived directly from the acoustic speed and density^{67,68}. We experimentally characterize and
175 measure the acoustic speed of our hydrogel. Firstly, with the acoustic speed of water being 1500
176 m/s and the distance between PZT and hydrophone positioned 20 mm apart in the water tank, the
177 time required for an acoustic pulse (time-of-flight, ToF) to travel from the transducer to the
178 hydrogel theoretically will be 13.3 μ s in free-field. Upon measurement of ToF with the hydrogel,
179 comparison of to the free-field measurement allows us to determine the time difference and the
180 acoustic speed through the hydrogel (**Fig. 3b**). The measured density of the hydrogel was 1166.7
181 kg/m³. Overall, the acoustic impedance of the hydrogel yielded 2.13 ± 0.11 MRayl and 2.17 ± 0.13
182 MRayl, with estimated acoustic speed of 1816 ± 76.36 m/s and 1864 ± 113.7 m/s on day 0 and day
183 7 respectively (**Fig. 3c, Supplementary Fig. 2**). Overall, the acoustic impedance of the
184 bioadhesive hydrogel remained stable across 7 days, with an average hydrogel impedance of 2.17
185 MRayl. Compared to the acoustic impedance of 1.99 MRayl for skin⁵², our bioadhesive hydrogel
186 exhibits a much more similar impedance to human skin compared to commercial ultrasound gels
187 such as Konix Sterile Gel and Aquasonic 100, indicating minimum acoustic loss of our hydrogel
188 in addition to its' long-term stability.

189 Further investigation of the long-term stability of the hydrogel in acoustic attenuation was
190 performed under low and high humidity conditions. Low humidity of 30% mimicked a typical
191 indoor room environment and 75% reflects high humidity outdoor conditions, which was emulated
192 by a sealed humidity controlled container storage where the hydrogel was stored^{69,70}. Our
193 hydrogel had an attenuation of up to 13% and less than 2% when stored in humidity conditions of
194 30% and 75% respectively over 35 days (**Fig. 3d-e**). Additionally, weight loss test was also
195 performed for both our hydrogel and a commercial gel stored in these two humidity conditions.
196 Under low humidity (RH 30%), our hydrogel exhibited a slow dehydration rate, retaining 76% of
197 its weight and remained stable post 7 days. Conversely, the weight of the commercial gel
198 significantly decreased with only 14% weight retention on day 7 (**Fig. 3f**). Under high humidity
199 (RH 75%), our hydrogel had a significant and consistent increase in weight of approximately 120%
200 after two weeks (**Fig. 3g**). Additional tests under room temperature and humidity conditions
201 exposure were also performed. Our hydrogel exhibits a slow dehydration rate, retaining ~65% of
202 its volume after 24 hours. In contrast, the commercial gel undergoes rapid dehydration, retaining

203 only ~63% volume after 3 hours and approximately 10% weight after 24 hours. After 24 hours,
204 the commercial gel is nearly fully dehydrated, whereas the hydrogel remains stable
205 (**Supplementary Fig. 3 and 4**). This suggests the potential of the self-recoverable and self-
206 rehydrating hydrogel properties within high humidity conditions.

207 To ensure long-term robustness in wearability, sufficient adhesion between SFAT-ACFAL
208 and the skin is necessary. Additionally, strong adhesion between the hydrogel and the PDMS-
209 based ACFAL is required aside from the interface between hydrogel and the skin to prevent
210 detachment. The robust integration between ACFAL and hydrogel was achieved by using the
211 photografting agent for the hydrogel. Treating PDMS with benzophenone (BZP), a type II
212 photoinitiator, extracts hydrogen from the grafted surface of PDMS and generates radicals
213 allowing the PDMS and hydrogel to form a polymeric bond under UV irradiation⁷¹ (**Fig. 3h**). As
214 a result, the adhesion of BZP-treated PDMS to the hydrogel was 2.09 N/cm, which was 13 times
215 higher than the adhesion of non-treated PDMS to the hydrogel (0.1513 N/cm) (**Fig. 3i**).
216 Optimization of the adhesiveness of our hydrogel to the skin was achieved by tuning the loading
217 of glycerol and was determined via measurement of adhesion force through 90° T-Peel test. As the
218 glycerol loading increases, the adhesion force of the hydrogel improves and plateaus when glycerol
219 loading exceeds 10 wt% (**Fig. 3j**). In this study, glycerol was loaded at 20 wt% to maintain high
220 water retention properties, allowing an adhesion force of ~0.941 N/cm, sufficient for attachment
221 to the skin. Skin adhesion cycling was performed subsequently to determine the adhesive
222 reusability, where adhesion force remained stable over 20 cycles with a mean adhesion force of
223 0.961 N/cm (**Fig. 3k**). Modulus compliance of hydrogel with skin was investigated, where the
224 modulus of the hydrogel is ~31.4 kPa, similar to that of skin tissues. Thus, providing minimal
225 mechanical mismatch and demonstrating suitability of skin-device interface (**Supplementary Fig.**
226 **5**)⁷². These results indicate that the bioadhesive hydrogel could provide an alternative to long-
227 term ultrasound applications.

228

229 **SFAT-ACFAL enables suppression of somatosensory evoked potentials at S1 targeting**

230 Studies in SEP by median nerve (MN) stimulation have been explored and researched
231 greatly. Well-defined characteristic morphology of EEG signals of SEP are distinguished into
232 waveform peaks assigned by their polarity (positive P or negative N) and its corresponding post-
233 stimulus latency (in ms)⁷³. The changes in latency and amplitudes of these waveform peaks are

234 often interpreted as dynamical alterations in neural activity because of combination from
235 peripheral and central nervous system to external stimulus. Specifically, early SEP peaks or “short
236 latency” SEPs occurring within 40 ms post-stimuli are of great importance as they have the least
237 variability in response to peripheral external stimulation whereas long latency responses are
238 susceptible to cognitive factors and higher ordered complex neural processing of the sensory
239 pathways⁷³. Thus, waveform peaks of N20, P27, N33, P50, N70, P100 and N140 were examined.
240 In brief, each of these peaks serve as a biomarker with implications of tactile information
241 processing. However, of most great interest corresponds to N20 (or commonly known as P27-N20
242 complex) has been highly known for its relevance to the sensory input of dorsal column-medial
243 lemniscal pathway and acts as a primary evoked response in response to peripheral stimuli to the
244 lateral portion hand area of somatosensory cortex extended posteriorly over to supramarginal
245 gyrus⁷⁴.

246 Recently, transcranial focused ultrasound stimulation at the somatosensory cortex has been
247 shown to suppress somatosensory evoked potential (SEP) via the elicitation of sensory stimuli.
248 The suppression in SEP effectively resulted in higher subjects’ ability to discriminate fine
249 differences in two points through sensory perception at the epidermis of distal phalanges⁵⁶. To
250 demonstrate the efficacy of our SFAT-ACFAL, we applied our device in targeting the left S1
251 through transmission of tFUS into the cortex at the CP3 site (**Fig. 4a**). Electroencephalographic
252 (EEG) electrodes using commercial Ag/AgCl was applied at the scalp of electrode sites CP1, C3,
253 P3, and CP5 in the 10-20 EEG configuration as a means to study the influence of tFUS short-to-
254 late onset evoked brain activity through understanding of changes in peak-to-peak amplitudes of
255 SEP complexes and spectral changes in power elicited by the contralateral (right) MN stimulation
256 with functional electrical stimulation (FES) (**Fig. 4b**).

257 To determine the efficacy in SEP suppression of our miniaturized transducer, we first
258 applied commercially available ultrasound gel coupled between the SFAT-ACFAL with the scalp
259 at the 10-20 EEG electrode site CP3. 650 kHz tFUS beams were pulsed to the target region (n =
260 5) with a pulse of 360 μ s ON and 640 μ s OFF at a pulse repetition frequency (PRF) of 1 kHz for
261 500 ms. The stimulation paradigm chosen has been demonstrated experimentally in humans to
262 suppress SEP⁵⁶ whilst ensuring minimal thermal heating effects with our device due to the short
263 pulse time (**Fig. 2g**). MN stimulation occurred for 200 μ s at 100 ms after the beginning of tFUS
264 transmission. Sham and tFUS treatment conditions were performed identically apart from the

265 device being turned off in the sham group. Some subjects reported auditory chirping noises initially
266 at the beginning of each trial produced by the device during stimulation. However, the chirping
267 noises quickly subsided within a few seconds reported by subjects. Additionally, subjects did not
268 report any discomfort, heating, or abnormal sensations at the site of tFUS treatment between sham
269 and tFUS treatments.

270 With our device for tFUS treatment, we demonstrated a significant decrease in short
271 latency peaks (P27-N20 complex) across electrode sites at C3 (sham, $0.289 \pm 0.083 \mu\text{V s.e.m.}$;
272 tFUS $0.086 \pm 0.073 \mu\text{V s.e.m.}$), P3 (sham, $0.803 \pm 0.221 \mu\text{V s.e.m.}$; tFUS $0.469 \pm 0.247 \mu\text{V}$
273 s.e.m.), and CP5 (sham, $0.222 \pm 0.056 \mu\text{V s.e.m.}$; tFUS $0.089 \pm 0.068 \mu\text{V s.e.m.}$) compared to the
274 sham. Conversely, no significant reduction in short latency peaks were observed at electrode site
275 CP1 (sham, $0.458 \pm 0.109 \mu\text{V s.e.m.}$; tFUS $0.266 \pm 0.038 \mu\text{V s.e.m.}$). tFUS using SFAT-ACFAL
276 did not produce any significant changes in long-latency peaks (**Fig. 4c-d, Supplementary Table**
277 **1-4**) but late potential (>140 ms) showed general attenuation across all electrodes in late-onset SEP
278 complexes.

279 Spectral decomposition of EEG signals enables understanding of spatial-temporal changes
280 in dynamics regarding excitation and inhibition of cortex in response to information
281 processing^{75,76}. Therefore, spectral analysis was performed on the grand averaged epochs of SEP
282 to evaluate the effects of tFUS using SFAT-ACFAL. By taking the difference between the spectral
283 decomposition of FUS and sham, a significant short latency decrease in alpha (7-12 Hz) and beta
284 (13-30 Hz) band power of -6 dB was observed within 100 ms of MN stimuli. Additionally, a short
285 period of low gamma band (30-50 Hz) power decrease was observed around 100 ms post MN
286 stimuli (**Supplementary Fig. 6**).

287

288 **Long-term wearability and neuromodulation of MiniUITra**

289 The ability for our device to stimulate the S1 region long-term was tested within the same
290 experimental protocols that target the characteristic pattern of SEP with MN stimuli. Particularly,
291 SEP suppression via tFUS tests were conducted in 3 sessions (Day 1, 7, and 28) throughout 28
292 days (**Fig. 5a**) to investigate the efficacy of neuromodulation using our MiniUITra device
293 (bioadhesive hydrogel incorporated) on healthy volunteers ($n = 4$). The length of the experimental
294 protocol was chosen to investigate the extreme longitudinal conditions of our MiniUITra device
295 over a month period, where our bioadhesive hydrogel remains stable compared to commercial gel

296 over 28 days (**Fig. 5b**). When MiniUITra was used on day 1, significant suppression of SEP was
297 observed compared to the sham group across all electrode channels. Furthermore, there was no
298 significant difference between the treatment group when our bioadhesive hydrogel was used
299 compared to commercial gel, validating the acoustic characteristics of the bioadhesive hydrogel in
300 ultrasound transmission has similar performance to commercially available ultrasound gel (**Fig.**
301 **5d**). Additional sessions were performed on day 7 and day 28, which also showed significant
302 suppression against the sham condition across all channels except for CP1 on day 7. We also
303 observe a general decrease in the P27-N20 complex over time. Overall, the SEP amplitude across
304 the epoch was observed with clear decreases in short (P27-N20 complex) and long latency (>70
305 ms) biomarkers (**Fig. 5c**). However, long latency biomarkers are more complex in its relation with
306 median nerve stimuli due to its association with indirect somatosensory pathways involving
307 cognitive and motor processes⁷⁷. Hence, the P27-N20 complex was focused due to its prominent
308 and well established association to contralateral stimuli at the S1 region^{78,79}. Results indicated
309 significant reduction in amplitude at the corresponding P27-N20 complexes across all electrode
310 channels over 28 days (**Fig. 5d**), demonstrating robustness in ultrasound neuromodulation over
311 long time stimulation with our MiniUITra.

312

313 **Discussion**

314 We have demonstrated a newly developed bioadhesive hydrogel coupled and miniaturized
315 wearable ultrasound transducer that offers long-term brain neuromodulation capability without the
316 need of handheld operators and fixtures. The device utilizes an alternative simplified
317 microfabrication approach without the need of standard lithography techniques for SFAT-ACFAL
318 patterning to achieve higher focality, acoustic intensity, and miniaturization. Additionally, our
319 development of a novel hydrogel provides mechanical compliance, bioadhesion and stable
320 acoustic coupling between our device and skin interface. For the first time, our hydrogel has shown
321 acoustic and adhesive stability for more than a month compared to current state-of-the-art acoustic
322 hydrogels stability of 72 hours. By integrating the two components, our device MiniUITra can be
323 used to perform noninvasive focused ultrasound stimulation delivered into the cortical region over
324 28 days with robust performance and clinical applications. Biosafety of the device was
325 demonstrated to achieve spatial pulsed averaged intensity and acoustic pressure within the safety

326 limits suggested by FDA guidelines and literature. Thus, our system provides a promising platform
327 for non-invasive long-term wearable ultrasound applications.

328 In conclusion, wearable ultrasound stimulation devices hold significant promise for the
329 long-term treatment of chronic diseases like Parkinson's disease, essential tremor, epilepsy and
330 depression. These devices offer non-invasive, spatiotemporal targeted modulation of neural
331 activity, potentially improving disease symptoms without the drawbacks of medications or
332 surgery. Their non-invasive nature and wearability also suggest the potential for home-based
333 therapy, although continued research is essential to optimize treatment protocols and ensure long-
334 term safety and efficacy across diverse patient populations.

335

336 **Methods**

337 **Fabrication of SFAT-ACFAL**

338 Geometric shape and radius of the ACFAL was determined first by selection of 10 mm
339 focal depth according to the equations governed by Fresnel lens⁸⁰, which was then implemented
340 into finite element analysis software for simulation (COMSOL Multiphysics 6.0, COMSOL Inc.).
341 Optimization of PDMS and air-cavity thickness was performed with reference to previous
342 feasibility of microfabrication (**Supplementary Fig. 7**)

343 Mold glass substrates were initially patterned by first laminating 36 um thick copper tape
344 (1125, 3M) onto adhesive interlayer (Ultra 582U, TransferRite), which was then laminated onto
345 an adhesive backing layer (GXF341, DigiClear Plus). The laminated copper tape was then
346 negatively patterned using laser etching (LPKF, U4 Laser) and transferred printed onto the glass
347 substrate (**Supplementary Fig. 8i**).

348 Patterned mold glass substrates were cleaned and prepared by first submerging into a
349 beaker filled with acetone and sonicated to remove particulates for 5 min. Substrates were then
350 removed, rinsed with distilled water and submerged in methanol for 5 min of sonication. The
351 substrates were then rinsed with distilled water before blow dried with purified nitrogen gas.
352 Substrate was spin-coated with a sacrificial layer (Omniccoat, Kayaku Advanced Materials) for 30s
353 at 1000 RPM and 3 min of planarization before soft-baking at 200°C on a hotplate. The parameters
354 were determined empirically through patterning and measurement of thickness using profilometer
355 (**Supplementary Fig. 8**) Subsequently, substrates were then spin-coated with 5 ml of PDMS
356 (Sylgard 184); prepared by mixing 1:10 of curing agent with base elastomer and desiccated for 1

357 hour at 500 RPM to achieve ~200 μm thickness and cured on a hotplate at 90°C for 35 mins.
358 Substrates were then placed in acetone filled beakers and sonicated for 5 min each to release the
359 patterned PDMS mold (**Supplementary Fig. 8ii**). Using tweezers, the patterned PDMS layer was
360 carefully removed and placed onto a temporary glass substrate, which was then trimmed with
361 medical scalpel. Similarly, the PZT (DL-47, Del Piezo) was subjected to the same substrate
362 cleaning process mentioned previously. 2 ml of prepared PDMS was spin-coated onto the surface
363 of PZT at 2000 RPM for 30s to achieve a thickness of 40 μm ; cured at 90 °C for 30 min
364 (**Supplementary Fig. 8iii**).

365 Next, the released patterned PDMS layer and coated-PDMS PZT was treated with Reactive
366 Ion Etching (RIE) O₂ plasma treatment for 25 s (30W @ 30% O₂, 30 SCCM) to remove organic
367 hydrocarbons on the surface and create silanol (SiOH) functional groups, effectively increasing
368 the wettability and rendering surface more hydrophilic⁸¹. The patterned PDMS layer was then
369 reversely bonded onto the coated-PDMS PZT by attachment and applying 1 kg weight
370 simultaneously on a 120 °C hotplate for 5 min (**Supplementary Fig. 8iv**).

371

372 **Acoustic Field Mapping of SFAT-ACFAL**

373 *Mapping.* The SFAT-ACFAL device was mounted on a submersible stand in a degassed distilled
374 glass water tank. Acoustic intensity and waveform were measured using a calibrated capsule
375 hydrophone (HGL-0200, Onda) mounted on a three-axis stage system, which was connected to an
376 oscilloscope (SDS 1204-XE, Siglent) via a signal preamplifier (AG-2010, Onda) interfaced to a
377 custom MATLAB program for automated 3D scanning and signal processing (**Supplementary**
378 **Fig. 9**). The device was controlled and actuated by a commercially available ultrasound system
379 (BBBoq, Image Guided Therapy Systems). Acoustic field scans without macaque skulls were first
380 performed at 500 μm increments (0 - 40 mm from transducer in a 40 mm x 40 mm grid workspace).
381 Focal depth and spatial peak locations were obtained from the acquired acoustic field scans axially
382 and radially. Subsequently, the macaque skull (3-mm thick macaque cortical bone, rehydrated for
383 24 h in phosphate buffer solution) was inserted in between the transducer and hydrophone using
384 the same scan procedures. Due to the curvature and inhomogeneous geometry, acoustic field scans
385 were performed at 500 μm increments (~10 - 40 mm from the transducer in a 40 mm x 40 mm grid
386 workspace) to avoid collision between transducer, skull, and hydrophone.

387

388 *tFUS Waveform.* Generation of tFUS profile from SFAT-ACFAL was performed using a 40-W
389 high-voltage biphasic ultrasound function generator system (BBBoq, Image Guided Therapy
390 System) controlled and pulsed by an external Arduino trigger. Briefly, the function generator was
391 set to deliver individual pulses at 360 μ s ON and 640 μ s OFF with center frequency of 650 kHz
392 (**Fig. 2e**). The Arduino was then programmed to trigger the function generator at a pulse repetition
393 frequency (PRF) of 1 kHz and pulse duration of 500 ms ON and 500 ms OFF.

394

395 *Electrical Characteristics.* SFAT-ACFAL was connected to an impedance spectrum analyzer
396 (SP300, BioLogic) using a two-electrode connection configuration. Impedance of the device was
397 measured from 0-1MHz to validate resonant frequencies. Fundamental harmonics and phases were
398 identified in addition to the desired 650kHz (**Figure 2h**).

399

400 *Thermal Heating.* SFAT-ACFAL was placed facing upwards on a 3D-printed mounted stand,
401 where the superficial side of the macaque skull was placed in contact with the transducer using
402 ultrasound coupling gel (Aquasonic 100, Parker). Three stimulation paradigms with varying duty
403 cycle and pulse duration were used (360 μ s ON/640 μ s OFF, 500 μ s ON/500 μ s OFF, 50ms
404 ON/50ms OFF) for 10 mins to compare and observe the thermal heating effects from tFUS (**Fig.**
405 **2f**). An infrared camera (One Edge, FLIR) was used to record three points in a triangular
406 configuration surrounding the targeting area on the inferior side of the macaque skull
407 (**Supplementary Fig. 1**).

408

409 **Synthesis and integration of bioadhesive hydrogel to SFAT**

410 *Materials and fabrication of bioadhesive hydrogel:* The preparation of the bioadhesive hydrogel
411 started with mixing the hydrogel solution. First, AMPS (Sigma-Aldrich) was dissolved in
412 deionized (DI) water at a 1:1 ratio using a vortex mixer for 30s. Subsequently, glycerol (Alfa
413 Aesar) with 20 wt% was added to the AMPS/DI water mixture using a vortex mixer for 30s. N,
414 N'-Methylenebis(acrylamide) (MBAA crosslinker, Sigma-Aldrich) with ~0.16 wt% was then
415 added and mixed for 60s. Irgacure 2959 (2-Hydroxy-4'-(2-hydroxyethoxy)-2-
416 methylpropiophenone 98%, Sigma-Aldrich) with ~0.59 wt%, serving as the photoinitiator, was
417 mixed for 30 s. The solution was stirred additionally for 30 minutes. To improve adhesion force
418 between PDMS and hydrogel, the PDMS-based ACFAL integrated with SFAT was treated with

419 benzophenone (BZP) by first mixing 10% w/w BZP with acetone for 60s via vortexing followed
420 by 60s of sonication to ensure complete incorporation of BZP in solvent. Subsequently, the
421 solution was pipetted onto the surface of PDMS and exposed to air for solution to evaporate for
422 10 min. Upon complete evaporation, the PDMS surface was washed gently with DI water three
423 times to remove excess BZP crystalline solids formed and dried with O₂ air gun before depositing
424 the bioadhesive hydrogel for curing. Lastly, bioadhesive hydrogel was integrated with SFAT-
425 ACFAL by cross-linking the hydrogel solution under UV light for 15 minutes (~4.21 J).

426

427 **Characterization of Bioadhesive hydrogel**

428 *Adhesion strength of bioadhesive hydrogel with skin and PDMS:* The adhesion strength of the
429 bioadhesive hydrogel was evaluated modified ASTM F2255-05 and ASTM F2256-05 methods
430 through custom-developed and integrated testing machine (FB5, Torbal) with 90°-peeling off test.
431 The samples were prepared with dimensions of 20 x 50 x 2 mm (width x length x thickness), and
432 the backside of each sample was affixed with Kapton film (7413D, 3M) to prevent stretching
433 during peeling. To measure the adhesion between the skin and bioadhesive hydrogel, the samples
434 were gently attached onto a skin, and then peeled off at a 90° angle from the skin at a speed of 68
435 mm/min. To measure the adhesion between PDMS and bioadhesive hydrogel, PDMS was initially
436 deposited and cured on a glass substrate mold (width: 50 mm, length: 76 mm). Then, a BZP
437 treatment process was conducted. Using a similar 90°-peeling off test, the substrate was mounted
438 and performed to compare adhesion force with and without BZP-treatment between the hydrogel
439 and PDMS (**Fig. 3i**).

440

441 *Weight Loss.* To measure the dehydration characteristics of the hydrogel, a weight loss test was
442 conducted. A circular-shaped bioadhesive hydrogel and a commercial gel (Aquasonic 100, Parker)
443 sample were prepared (diameter: 19 mm, thickness: 1 mm). The weight of each was measured over
444 time both in a typical room environment (~41%, ~23 °C) and inside a container with high humidity
445 (~65%, ~23 °C) (**Supplementary Fig. 10**). The weight loss of the samples (W_i) was calculated
446 using the equation $W_i (\%) = (W_t - W_i) / W_i \times 100$, where W_i and W_t denote, respectively, the initial
447 weight of the sample and the weight of the sample at different times.

448

449 *Acoustic characteristics of hydrogel.* Acoustic properties of the bioadhesive hydrogel were
450 characterized by measuring and estimating the acoustic time-of-flight difference of ultrasound
451 transmission through water, PET, and hydrogel between transducer and hydrophone. A single
452 cycle sine wave pulse was generated using a 3-level beamformer transmitter circuit (TX7316,
453 Texas Instrument) with a supplied driving voltage of ± 20 V. To measure the acoustic time-of-
454 flight of the hydrogel, a 3-mm thick hydrogel was prepared with a mold consisting of PET film
455 and Ecoflex frame (**Supplementary Fig. 11**) and measurements were performed over a period of
456 7 days. The purpose of the Ecoflex frame was to maintain the thickness of the hydrogel and to
457 prevent the penetration of the water into the hydrogel when measuring in the water tank. Between
458 measurements, the Ecoflex frame was removed temporarily, and the hydrogel samples were stored
459 in a room environment (humidity: $\sim 30\%$, temperature: $\sim 23^\circ\text{C}$). Then, when measurements were
460 taken again, the Ecoflex frame was placed around the hydrogel again to prevent water from
461 entering the hydrogel. The acoustic time-of-flight was measured by placing the hydrogel samples
462 between transducer and hydrophone in a water tank. The acoustic speed of the hydrogel was
463 estimated by following equations⁵²:

$$464 \quad c_{hydrogel} = \frac{T_{hydrogel} + 2T_{PET}}{\left(\frac{T_{hydrogel} + 2T_{PET}}{c_{water}}\right) - \frac{2T_{PET}}{c_{PET}} - \Delta t_{PET} + \Delta t_{PET+Hydrogel}}$$

465 Where $T_{Hydrogel}$ is the thickness of the bioadhesive hydrogel, T_{PET} is the thickness of the PET film,
466 c_{Water} is the speed of sound in water (1500 m/s), c_{PET} is the speed of sound in PET film
467 (polyethylene, high density: 2430 m/s,⁸²), ΔT_{PET} is ToF difference between with and without PET
468 film, $\Delta T_{PET+Hydrogel}$ is ToF difference between with and without hydrogel samples.

$$469 \quad Z_{Hydrogel} = \rho_{Hydrogel} \times c_{Hydrogel}$$

470 Where $Z_{Hydrogel}$ is the acoustic impedance of the bioadhesive hydrogel, $\rho_{Hydrogel}$ is the density of
471 the hydrogel, $c_{Hydrogel}$ is the speed of sound of the hydrogel.

472
473 *Long-term acoustic stability:* To assess the long-term acoustic stability of the bioadhesive
474 hydrogel, the ultrasound intensity of the bioadhesive hydrogel integrated SFAT was measured over
475 time. The number of circular-shaped hydrogels were prepared and stored in a container with high
476 humidity ($\sim 65\%$, $\sim 23^\circ\text{C}$). At specific time intervals, each bioadhesive hydrogels were taken out of
477 the container and attached to a bare PZT transducer. All measurements were conducted under the
478 deionized water. To prevent rapid swelling of the AMPS-based bioadhesive hydrogel upon contact

479 with water, bioadhesive on the bare PZT transducer was covered with a thin Ecoflex cap
480 (thickness: 0.5 mm). Then, the attenuation of ultrasound intensity due to the bioadhesive hydrogel
481 over time was measured using a custom setup 3-axis hydrophone acoustic scanning system.

482

483 **Device Integration of MiniUITra**

484 Fabricated SFAT-ACFAL was connected via low temperature solder (NP510-LT HRL1, Kester)
485 to a BNC cable and housed in a custom-designed 3D printed casing (PLA Galaxy, Prusa), which
486 was lined with copper shielding (1181, 3M) and grounded to the BNC shielding layer for
487 electromagnetic shielding purposes. To integrate SFAT-ACFAL with the bioadhesive hydrogel,
488 The hydrogel solution was then poured to a thickness of 1 mm. Subsequently, the bioadhesive
489 hydrogel on the SFAT-ACFAL was cross-linked under UV light for 15 minutes. Finally, the
490 integrated device was completed by removing the mold (**Supplementary Fig. 8**).

491

492 **Characterization of tFUS on sensory-evoked potentials in S1 using SFAT-ACFAL**

493 *Participants.* The Institutional Review Board (IRB) at University of Texas at Austin approved all
494 experimental procedures under the study (STUDY00003279). Five healthy volunteers (4 male, 1
495 female, aged 24-36 with a mean age of 27.4 ± 5.1 years) provided written informed consent to
496 participate in the study. Volunteers were screened for contraindications and neurological
497 impairment and all subjects were right-hand dominant.

498

499 *Experimental setup.* Participants were positioned and seated in an adjustable height chair, where
500 their right forearm is fully extended and supported in supination. Four 10-20 EEG electrode sites
501 (C3, CP1, P3, CP5) were connected for recording somatosensory evoked potentials. During
502 testing, subjects were initially stimulated by FES with varying currents (8-25 mA, 200 μ s) to obtain
503 the minimum threshold necessary to elicit muscle contraction of the right contralateral side. The
504 SFAT-ACFAL was applied topically to CP3 manually with administration of ultrasound gel
505 (Aquasonic 100, Parker) as interface to the scalp, which was then held in place using medical tape.
506 Additionally, three electrical stimulation electrodes (2" Round, Reserv) were placed on the right
507 contralateral arm (ground electrode on elbow, bipolar electrodes axially paired on the wrist via
508 palpation of median nerve). The electrodes were connected to a functional electrical stimulation

509 (FES) system (RehaMove3, Hasomed) for median nerve stimulation (MN), which was controlled
510 externally by custom Python software.

511 tFUS treatment condition stimulation occurring 100 ms before MN stimuli (360 μ s ON and
512 640 μ s OFF, PRF 1kHz, Pulse Duration 500ms ON 500ms OFF) was controlled by programming
513 of microcontroller (Uno, Arduino), which was connected to trigger the ultrasound generator
514 (BBBoq, Image Guided Therapy System), FES system (MN stimuli), and EEG amplifier for time-
515 locked epoch events during somatosensory evoked potentials (SEP) (**Supplementary Fig. 12**).
516 Custom Python code was developed to integrate all systems together in addition to use of
517 LabStreamingLayer (LSL) to stream and log EEG data into dataframe with external data including
518 trigger and metadata. Subjects were then subjected to three blocks of trials, where each block
519 consisted of four trials (FUS-/FES-, FUS-/FES+, FUS+/FES-, FUS+/FES+) and each trial lasted
520 3 mins. Within each trial, 30 s of baseline recording occurs before 120 s of sham/FUS followed by
521 30s of rest recording to ensure sufficient buffered data for post-recording cleaning. Total recording
522 session time was approximately 1 h.

523
524 *Electroencephalography.* Subjects recruited were invited to a dedicated EEG recording room with
525 minimal electronics for minimizing electromagnetic interferences. Tape ruler was used to measure
526 the distance between nasion-to-inion and left-right preauricular points to determine electrode
527 positioning according to the 10-20 system for EEG recording. Marker was used to indicate the
528 position of C3, CP1, P3, CP5 for EEG and CP3 for tFUS targeting (**Fig. 4b**). Subsequently, rubbing
529 alcohol was applied carefully at the sites before conductive hydrogel electrodes (H124SG,
530 Kendall) were applied carefully to the scalp to ensure minimal obstruction of hair. Impedance per
531 electrode was measured using commercial amplifier (eego MyLab, AntNeuro) to ensure it is less
532 than 10k Ω . EEG data were digitized at 512 Hz and stored for offline analysis.

533
534 *Statistical analysis of somatosensory evoked potentials.* Digitized EEG data were analyzed offline
535 by first filtering using a third-order butterworth bandpass filter (2-90 Hz) followed by a first-order
536 butterworth bandstop filter (59-61 Hz) to remove DC offsets, mains interference, and high
537 frequency noises. A total of 120 epochs per trial recorded was then extracted using custom
538 MATLAB code using triggered signals as markers. Briefly, data were epoched around median
539 nerve stimulus trigger, 200ms prior up to 500 ms after the trigger was extracted as a single epoch

540 for analysis. Subsequently, the data was baseline corrected by subtracting the mean values from =
541 -200 ms to 0 ms. For each epoch, inspection of artifacts using rejection criteria of absolute peak-
542 to-peak amplitude threshold greater than 75 μ V will be removed. Grand averaged epochs across 5
543 subjects and 15 trials were obtained to determine the effects of sham and FUS in SEP using SFAT-
544 ACFAL elicited by MN stimuli. EEG biomarkers N20, P27, N33, P50, N70, P100, and N140 were
545 extracted by obtaining the mean amplitude \pm 2 ms the desired biomarker time event due to the
546 difficulty to reliably identify SEP peaks accurately per trial. Statistical analyses were performed
547 on mean peak-to-peak amplitudes for the N20/P27, N33/P27, P50/N33, N70/P50, P100/N70,
548 N140/P100 and long potential (LP) components (**Supplementary Table 1-4**). These data were
549 averaged across all trials and subjects and presented as mean \pm s.e.m for different group conditions.
550 Non-parametric statistical test using Wilcoxon signed-rank test was applied for SEP complexes to
551 determine significance of treatment conditions.

552

553 *Spatial-Temporal Analysis.* Spatial-temporal frequency analysis was performed (MATLAB
554 R2021a, The MathWorks) to decompose effects and changes in frequency spectrum due to S1
555 targeting using tFUS with SFAT-ACFAL as a function of time⁸³. Short-time Fourier transform
556 (STFT) was used with a window size of 4.8 ms and 2.3 ms overlap through Hamming window
557 approach. Power of spectral data was then converted into power (dB). Comparison between
558 treatment groups was performed by subtracting spectral epochs to observe dynamic changes in
559 power with respect to frequency bands, where -3 dB and -6 dB corresponds to one-fold and two-
560 fold decrease respectively (**Supplementary Fig. 6**).

561

562 **Long-term demonstration of tFUS neuromodulation of MiniUITra**

563 *Participants.* The Institutional Review Board (IRB) at University of Texas at Austin approved all
564 experimental procedures under the study (STUDY00003279). Four healthy volunteers (4 male,
565 aged 27-36 with a mean age of 32.5 ± 4.7 years) provided written informed consent to participate
566 in the study. Volunteers were screened for contraindications and neurological impairment and all
567 subjects were right-hand dominant.

568

569 *Experimental setup.* Subjects were invited to S1 targeted tFUS stimulation using SFAT-ACFAL
570 for long-term study (Day 1, 7, and 28). For each session, subjects were pre-screened for

571 contraindications before beginning the experiment. Four 10-20 EEG electrode sites (C3, CP1, P3,
572 CP5) were connected for recording somatosensory evoked potentials (**Fig. 4b**). Minimum
573 threshold for right contralateral hand movement due to MN stimulation was performed to obtain
574 the minimum threshold necessary to elicit muscle contraction of the right contralateral side. The
575 SFAT-ACFAL with bioadhesive hydrogel was applied to CP3 and held in place independently by
576 its adhesive nature. For EEG recording stability, additional medical tape was used to fix EEG
577 electrodes and transducers to prevent motion artifacts. Three electrical stimulation electrodes (2”
578 Round, Reserv) were placed on the right contralateral arm similarly to the previous experiment for
579 S1 targeting mentioned before. The electrodes were connected to a functional electrical stimulation
580 (FES) system (RehaMove3, Hasomed) for MN stimulation.

581 tFUS treatment and sham conditions performed identically with the exception of subjects
582 subjected to five blocks of trial, where each block consisted of two trials (FUS-/FES+; Sham,
583 FUS+/FES+; Treatment) and each trial lasted 3 mins. Total recording session time was
584 approximately 1 h.

585
586 *Statistical analysis of somatosensory evoked potentials.* A total of 120 epochs per trial recorded
587 was then extracted using custom MATLAB code using triggered signals as markers. Grand
588 averaged epochs across 4 subjects and 20 trials were obtained to determine the effects of sham and
589 FUS in SEP using SFAT-ACFAL elicited by MN stimuli. EEG biomarkers N20 and P27 were
590 extracted by obtaining the mean amplitude ± 2 ms the desired biomarker time event due to the
591 difficulty to reliably identify SEP peaks accurately per trial. Statistical analyses were performed
592 on mean peak-to-peak amplitudes for the N20/P27. These data were averaged across all trials and
593 subjects and presented as mean \pm s.e.m for different group conditions. Two-way ANOVA was
594 applied for SEP complexes to determine significance of treatment conditions across days with
595 treatment (hydrogel) and with control (commercial gel) in comparison to sham (no FUS)
596 conditions within groups.

597
598 *Study approval.* All experiments were performed in compliance with the Institutional Review
599 Board with approval at the University of Texas at Austin (STUDY00003279).

600

601 *Code availability.* The codes used for this study are available on GitHub at
602 <https://github.com/kevintang725/MiniUITra-LSL>.

603

604 **Acknowledgements**

605 We thank Wynn Legon, Greg Fonzo, José del R. Millán, Samantha Santacruz and Yaoyao Jia for
606 the discussions and advice. We would like to thank Nanshu Lu for her guidance and providing
607 access to the use of the LPKF Protolaser U4 system. We would like to thank José del R. Millán
608 for providing access to the RehaMove3 FES system. H.W. would like to acknowledge support
609 from Alzheimer's Association New to the Field (AARG-NTF) research grant, University of Texas
610 at Austin Startup Fund, and NIH Maximizing Investigators' Research Award (MIRA) (R35) grant.
611 J.J would like to acknowledge support from the Human Frontier Science Program (HFSP)
612 Fellowship. We acknowledge BioRender.com for the figures drawing.

613

614 **Author Contributions**

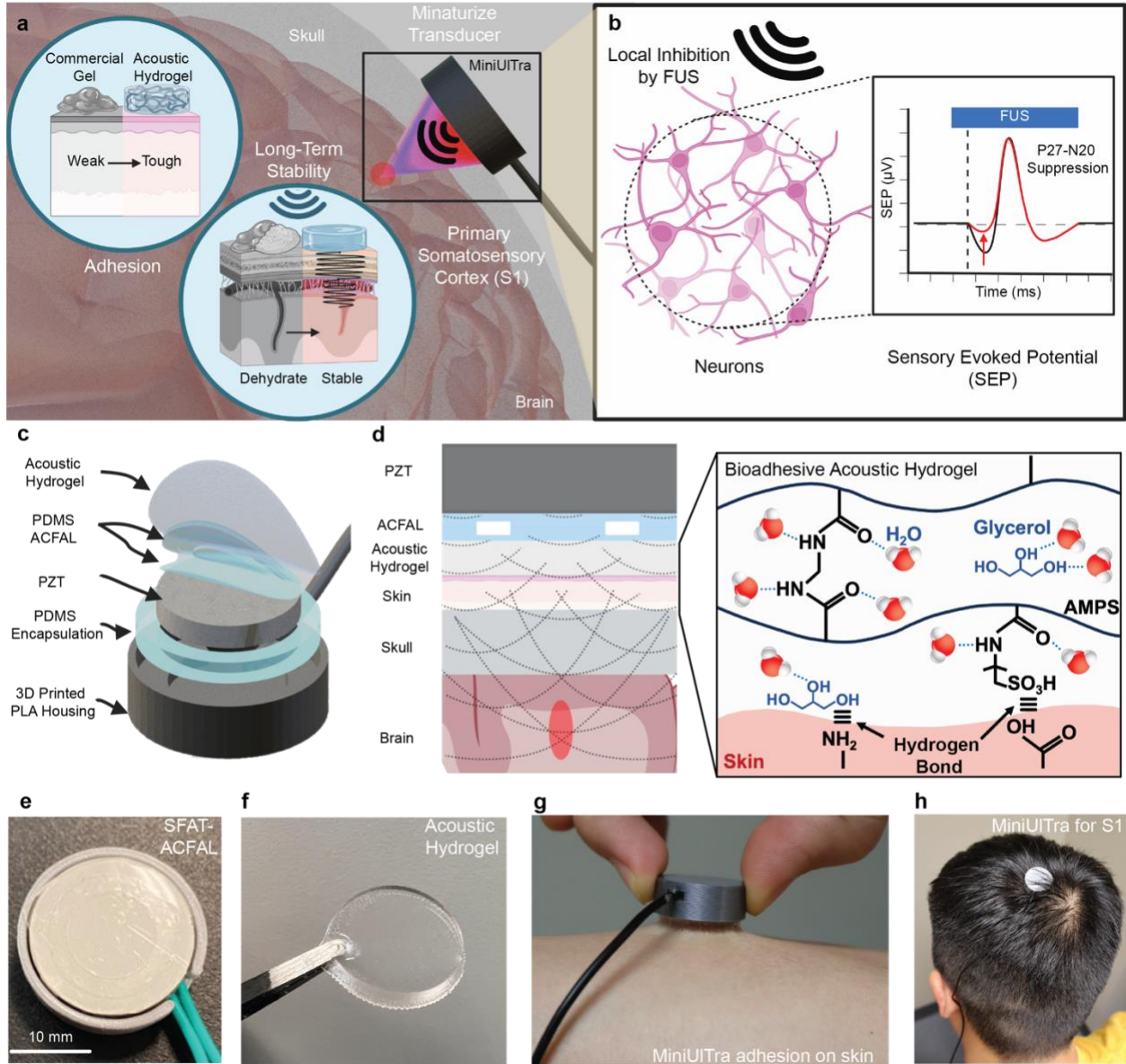
615 Conceptualization: K.W.K.T., J.J., and H.W.; Methodology: K.W.K.T. and J.J.; Software:
616 K.W.K.T.; Validation: K.W.K.T. and J.J.; Formal Analysis: K.W.K.T. and J.J.; Investigation:
617 K.W.K.T., J.J., J-C.H., and M.M.Y.; Data Curation: K.W.K.T. and J.J.; Writing - Original Draft:
618 K.W.K.T. and J.J.; Writing - Review & Editing: K.W.K.T., J.J., H.D., W.W., X.L., I.P., M.M.Y.,
619 W.H., W.D.M.B., A.R.L., B.A., and H.W.; Visualization: K.W.K.T. and J.J.; Project
620 Administration: K.W.K.T and H.W.; Resources: N.L. and H.W.; Funding: H.W.

621

622 **Conflict of Interest**

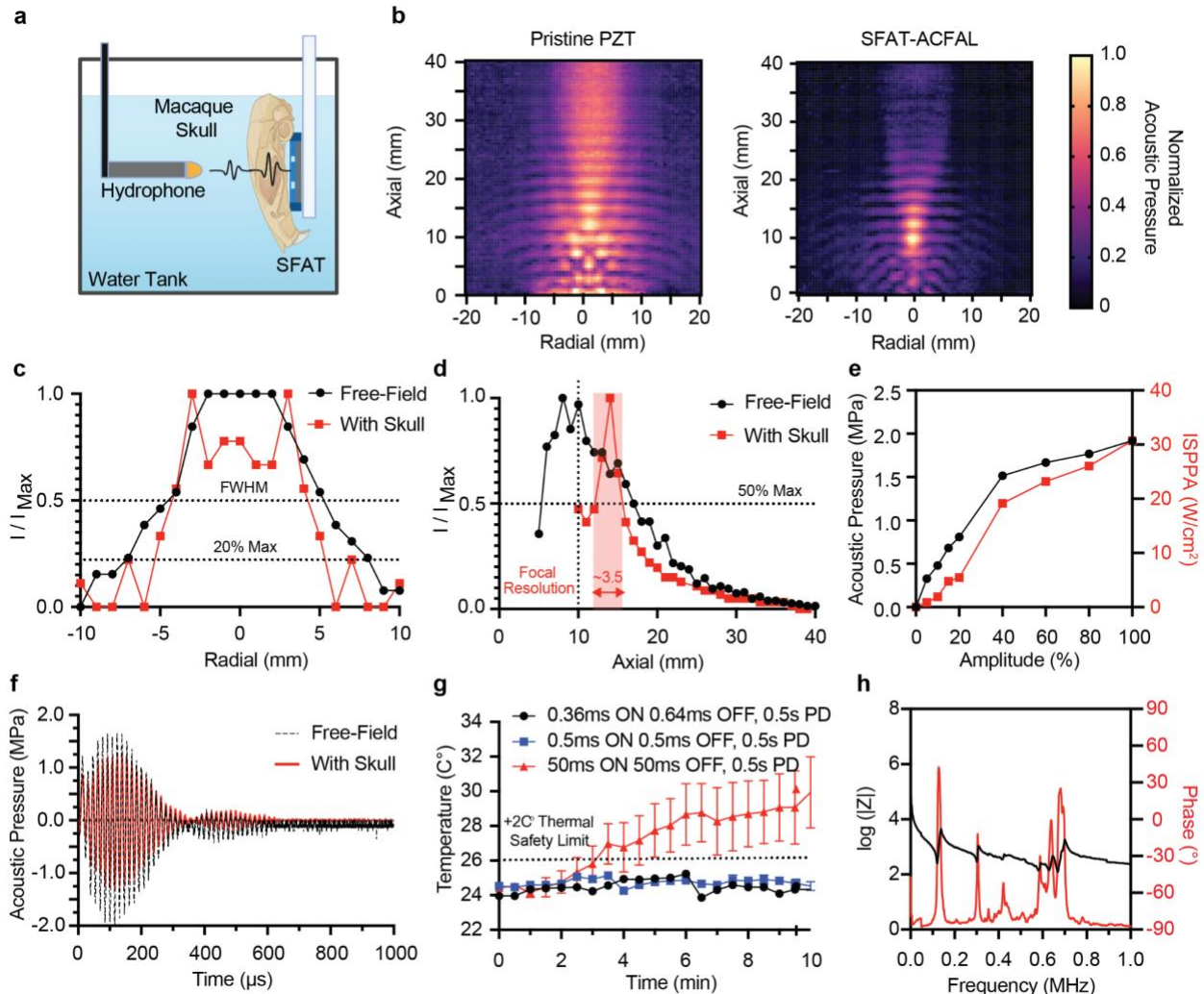
623 The authors declare the following competing financial interest(s): A patent application relating to
624 this work has been filed.

625 **Figures**



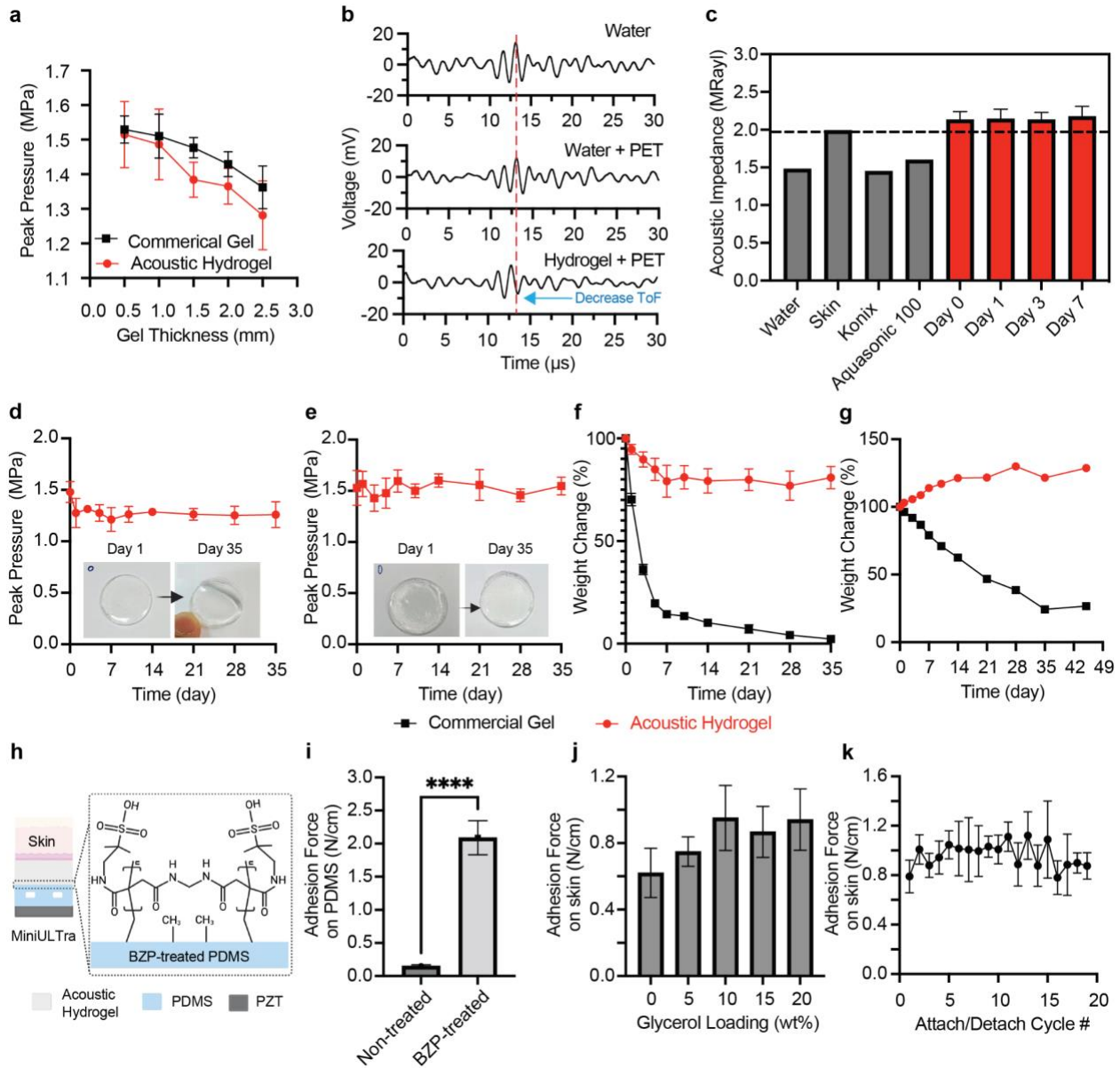
626
 627 **Figure 1. Miniaturized and Bioadhesive-Coupled Ultrasound Transducer (MiniUITra).** a)
 628 Illustration of MiniUITra that continuously adheres to the scalp targeting the primary
 629 somatosensory cortex (S1) with high adhesion force, low acoustic attenuation and miniaturized
 630 transducer. b) Mechanism of suppression of P27-N20 complex in somatosensory evoked potential
 631 (SEP) through focused ultrasound stimulation locally at the S1. c) Schematic of layered structure
 632 of MiniUITra that assembles the piezoelectric with PDMS-based ACFAL and bioadhesive
 633 hydrogel integrated into a compact 3D-printed housing. d) Side-view of layered schematic
 634 including chemical structure of bioadhesive hydrogel and its' adhesion mechanisms e-f) Optical

635 images of design and fabricated SFAT-ACFAL and bioadhesive hydrogel. **g)** Adhesion of
 636 MiniUITra on skin. **h)** Demonstration of MiniUITra on the scalp for S1 targeted neuromodulation.



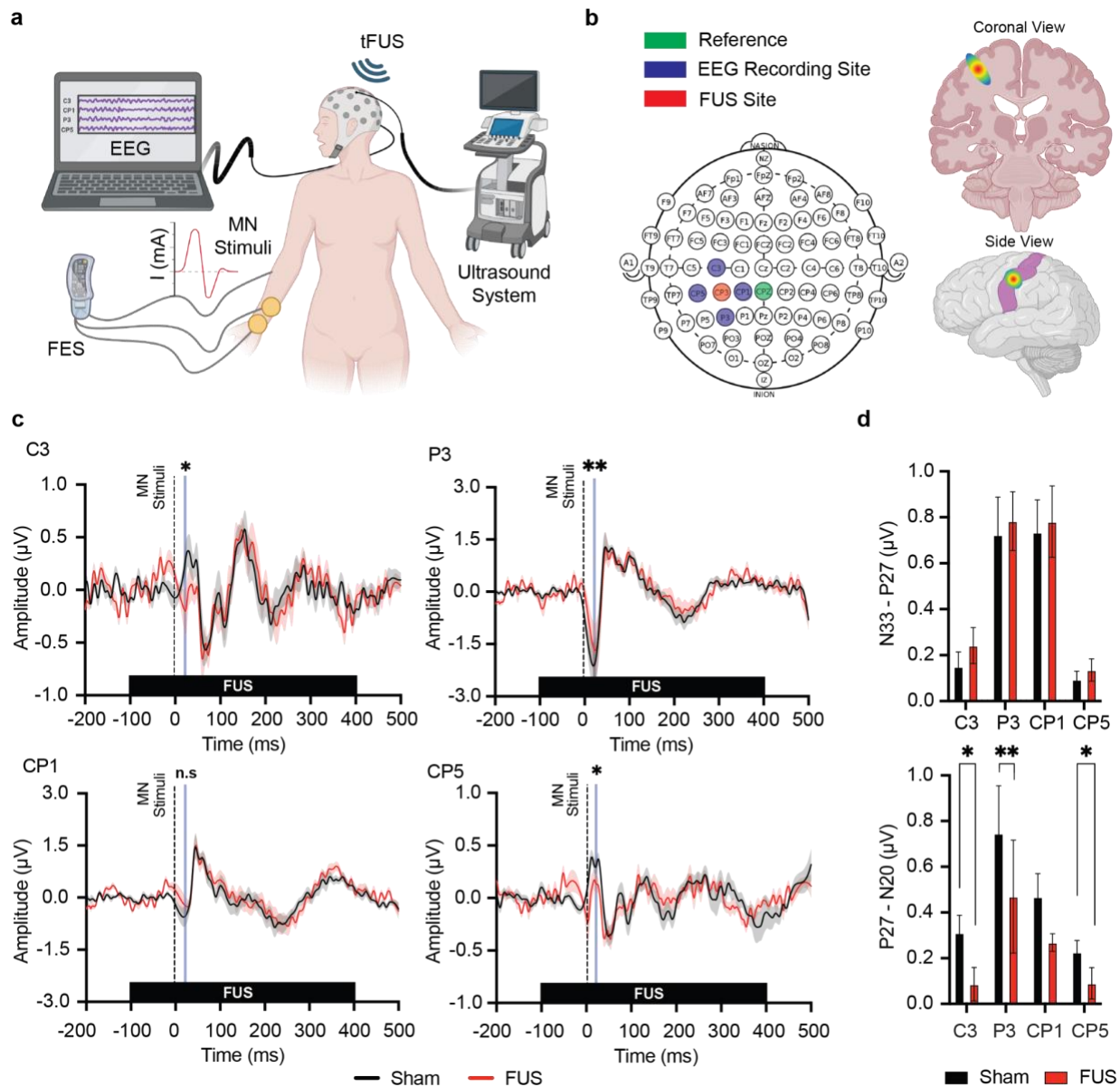
637
 638 **Figure 2. Self-Focusing Acoustic Transducer (SFAT) using Air-Cavity Fresnel Lens**
 639 **(ACFAL).** **a)** Schematic of experimental setup for characterization of SFAT-ACFAL. **b)**
 640 Comparison of acoustic field distribution and intensity with Pristine PZT (left) and with PDMS-
 641 based ACFAL (right). **c)** Normalized radial acoustic intensity profile in free-field and with the
 642 presence of a macaque skull at focal depth 10 mm. **d)** Normalized uniaxial acoustic intensity
 643 profile in free-field and with the presence of a macaque skull. **e)** Acoustic pressure (MPa) and
 644 intensity ($ISPPA$) calibration curve measured when SFAT-ACFAL at varying driving amplitude
 645 using ultrasound generator system. **f)** Measured waveform of ultrasound pulse using stimulation
 646 paradigm of 360 μ s with and without macaque skull. **g)** Thermal effect of SFAT-ACFAL on macaque

647 skull measured with infrared camera on varying stimulation parameters. **h)** Electrical impedance
 648 and phase of SFAT-ACFAL.



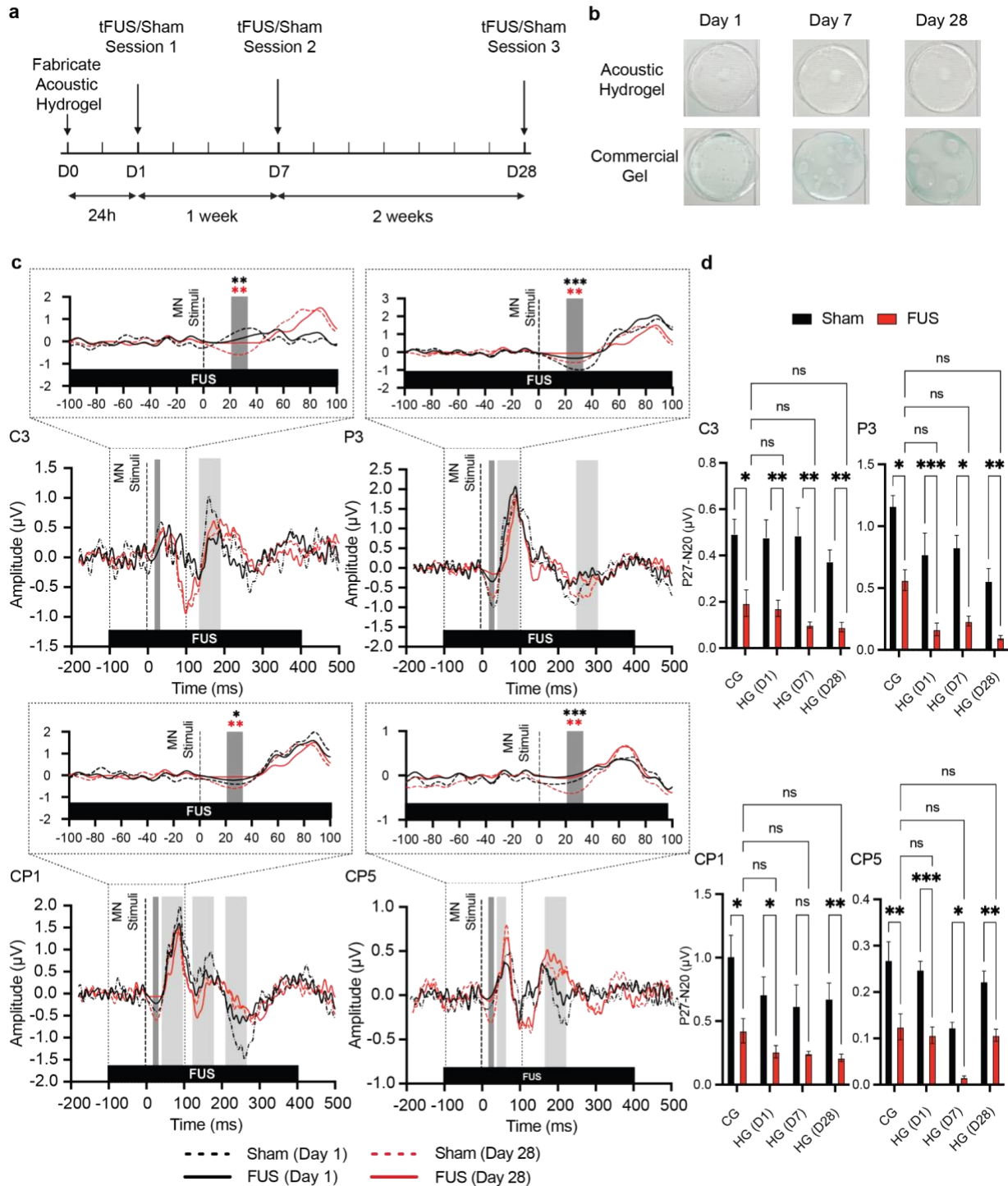
649
 650 **Figure 3. Bioadhesive hydrogel.** **a)** Comparison of ultrasound intensity decreases according to
 651 thickness changes in bioadhesive hydrogel and commercial gel (Aquasonic 100, Parker), (n = 6
 652 for each thickness). **b)** Comparison of acoustic time-of-flight (ToF) for ultrasound transmission
 653 through water, PET, and hydrogel. **c)** Acoustic impedance of the hydrogel for 7 days (n = 4 each
 654 day) compared to commercial gel, water, and human skin. **d)** Peak-pressure attenuation of
 655 bioadhesive hydrogel under 30% humidity and 22°C over 35 days. (n = 4). **e)** Peak-pressure
 656 attenuation of bioadhesive hydrogel under 75% humidity and 22°C over 35 days. (n= 4). **f)** Weight

657 change of the bioadhesive hydrogel and commercial gel in the room environment (humidity:
 658 ~30 %, temperature: ~22 °C, n = 4). **g)** Weight change of the bioadhesive hydrogel and commercial
 659 gel with high humidity (humidity: ~75 %, temperature: ~22°C, n = 4). **h)** Chemical structure of
 660 the bioadhesive hydrogel integrated ACFAL by grafting the bioadhesive hydrogel to
 661 benzophenone (BZP) treated PDMS. **i)** Improvement of adhesion force with BZP-treated PDMS
 662 (n = 4). **j)** Adhesion force of the bioadhesive hydrogel according to glycerol loading change (n =
 663 5). **k)** Adhesion force of the 20-cycle attachment/detachment test of the bioadhesive hydrogel on
 664 skin (n=4).



665

666 **Figure 4. Evaluation of neuromodulation in somatosensory evoked potential using SFAT-**
667 **ACFAL. a)** Schematic representation of experimental setup. **b)** Illustration of EEG electrode and
668 SFAT-ACFAL placement in 10-20 EEG montage with its corresponding targeting of left S1 with
669 FUS at CP3. **c)** Grand average of epochs where median nerve (MN) stimulation occurs at $t = 0$ ms
670 and FUS or sham begins at $t = -100$ ms (red line indicates SEP under FUS+, black line indicates
671 SEP under sham, highlighted blue indicates where significant difference was observed P27-N20
672 complex in SEP). **d)** Summary of effect of FUS compared to sham in P27-N20 and N33-P27
673 complexes of SEP. Suppression of early onset P27-N20 complex observed across C3, P3, and CP5
674 in SEP by FUS ($n=5$ per group, Wilcoxon signed-rank test, 4 male and 1 female). All plots show
675 mean \pm s.e.m unless otherwise mentioned, * $P < 0.05$, ** $P < 0.01$, and *** $P < 0.001$.



676

677 **Figure 5. Long-term suppression of the P27-N20 complex in somatosensory evoked-potential**

678 **(SEP) using MiniUITra.** **a)** Long-term experimental protocol for evaluating efficacy of hydrogel.

679 The hydrogel was fabricated a day before the first session (D0). Three sessions per subject, each

680 consisting of 10 trials of 3 minutes, each trial consisting of 120 epochs (tFUS/Sham) on day 1

681 (D0), 7 (D7) and 28 (D28). Each subject had their personal hydrogel with the device, which was

682 stored in room temperature and ~30% humidity. **b)** Optical image of prepared hydrogel compared
683 to commercial ultrasound gel with the corresponding sessions. **c)** Grand average epochs comparing
684 effects of sham and FUS with median nerve (MN) stimulation on SEP across days 1, 7 and 28
685 using hydrogel. MN stimulation occurs at $t = 0$ ms and FUS or sham begins at $t = -100$ ms (black
686 solid line indicates SEP under FUS+ on day 1; black dashed line indicates SEP under Sham on day
687 1; red solid line indicates SEP under FUS+ on day 28; red dashed line indicates SEP under Sham
688 on day 28; highlighted dark gray indicates where significant difference was observed P27-N20
689 complex in SEP; highlighted light gray indicates where observable differences in long latency
690 complexes). **d)** Suppression of early onset P27-N20 complex observed across C3, CP1, and CP5
691 in SEP by FUS shown within each group. No significant difference was observed across FUS
692 groups in bioadhesive hydrogel (HG) when compared to the FUS group using commercial gel
693 (CG). Significant decrease in P27-N20 complexes was observed when comparing within each day
694 of the hydrogel. ($n = 4$ per group, Two-Way Anova, 4 male). All plots show mean \pm s.e.m unless
695 otherwise mentioned, * $P < 0.05$, ** $P < 0.01$, and *** $P < 0.001$.

696 **References**

- 697 1. Marras, C. *et al.* Prevalence of Parkinson's disease across North America. *npj Parkinson's*
698 *Disease* **4**, 1–7 (2018).
- 699 2. Matthews, K. A. *et al.* Racial and ethnic estimates of Alzheimer's disease and related
700 dementias in the United States (2015–2060) in adults aged ≥ 65 years. *Alzheimers. Dement.*
701 **15**, 17–24 (2019).
- 702 3. Visser-Vandewalle, V. *et al.* Deep brain stimulation for obsessive–compulsive disorder: a
703 crisis of access. *Nat. Med.* **28**, 1529–1532 (2022).
- 704 4. Mar-Barrutia, L. *et al.* Deep brain stimulation for obsessive-compulsive disorder: A
705 systematic review of worldwide experience after 20 years. *World J Psychiatry* **11**, 659–680
706 (2021).
- 707 5. Volkmann, J. Deep brain stimulation for the treatment of Parkinson's disease. *J. Clin.*
708 *Neurophysiol.* **21**, 6–17 (2004).
- 709 6. Benabid, A. L. Deep brain stimulation for Parkinson's disease. *Curr. Opin. Neurobiol.* **13**,
710 696–706 (2003).
- 711 7. Deuschl, G. *et al.* A randomized trial of deep-brain stimulation for Parkinson's disease. *N.*
712 *Engl. J. Med.* **355**, 896–908 (2006).
- 713 8. Flora, E. D., Perera, C. L., Cameron, A. L. & Maddern, G. J. Deep brain stimulation for
714 essential tremor: a systematic review. *Mov. Disord.* **25**, 1550–1559 (2010).
- 715 9. Blomstedt, P., Hariz, G.-M., Hariz, M. I. & Koskinen, L.-O. D. Thalamic deep brain
716 stimulation in the treatment of essential tremor: a long-term follow-up. *Br. J. Neurosurg.*
717 (2007) doi:10.1080/02688690701552278.
- 718 10. Baizabal-Carvallo, J. F., Kagnoff, M. N., Jimenez-Shahed, J., Fekete, R. & Jankovic, J. The
719 safety and efficacy of thalamic deep brain stimulation in essential tremor: 10 years and

- 720 beyond. *J. Neurol. Neurosurg. Psychiatry* **85**, 567–572 (2014).
- 721 11. Hubble, J. P. *et al.* Deep brain stimulation for essential tremor. *Neurology* **46**, 1150–1153
722 (1996).
- 723 12. Koller, W. C., Lyons, K. E., Wilkinson, S. B., Troster, A. I. & Pahwa, R. Long-term safety
724 and efficacy of unilateral deep brain stimulation of the thalamus in essential tremor. *Mov.*
725 *Disord.* **16**, 464–468 (2001).
- 726 13. Li, M. C. H. & Cook, M. J. Deep brain stimulation for drug-resistant epilepsy. *Epilepsia* **59**,
727 273–290 (2018).
- 728 14. Loddenkemper, T. *et al.* Deep brain stimulation in epilepsy. *J. Clin. Neurophysiol.* **18**, 514–
729 532 (2001).
- 730 15. Boon, P. *et al.* Deep Brain Stimulation in Patients with Refractory Temporal Lobe Epilepsy.
731 *Epilepsia* **48**, 1551–1560 (2007).
- 732 16. Theodore, W. H. & Fisher, R. S. Brain stimulation for epilepsy. *Lancet Neurol.* **3**, 111–118
733 (2004).
- 734 17. Cury, R. G. *et al.* Thalamic deep brain stimulation for tremor in Parkinson disease, essential
735 tremor, and dystonia. *Neurology* **89**, 1416–1423 (2017).
- 736 18. Vercueil, L. *et al.* Deep brain stimulation in the treatment of severe dystonia. *J. Neurol.* **248**,
737 695–700 (2001).
- 738 19. Vidailhet, M. *et al.* Bilateral deep-brain stimulation of the globus pallidus in primary
739 generalized dystonia. *N. Engl. J. Med.* **352**, 459–467 (2005).
- 740 20. Denys, D. *et al.* Deep brain stimulation of the nucleus accumbens for treatment-refractory
741 obsessive-compulsive disorder. *Arch. Gen. Psychiatry* **67**, 1061–1068 (2010).
- 742 21. Hariz, M. I. Complications of deep brain stimulation surgery. *Mov. Disord.* **17 Suppl 3**,

- 743 S162-6 (2002).
- 744 22. Salatino, J. W., Ludwig, K. A., Kozai, T. D. Y. & Purcell, E. K. Glial responses to
745 implanted electrodes in the brain. *Nat Biomed Eng* **1**, 862–877 (2017).
- 746 23. A visual and narrative timeline of US FDA milestones for Transcranial Magnetic
747 Stimulation (TMS) devices. *Brain Stimul.* **15**, 73–75 (2022).
- 748 24. Elahi, B., Elahi, B. & Chen, R. Effect of transcranial magnetic stimulation on Parkinson
749 motor function—Systematic review of controlled clinical trials. *Mov. Disord.* **24**, 357–363
750 (2009).
- 751 25. Noninvasive brain stimulation in Alzheimer’s disease: Systematic review and perspectives
752 for the future. *Exp. Gerontol.* **46**, 611–627 (2011).
- 753 26. McNamara, B., Ray, J. L., Arthurs, O. J. & Boniface, S. Transcranial magnetic stimulation
754 for depression and other psychiatric disorders. *Psychol. Med.* **31**, 1141–1146 (2001).
- 755 27. Richter, L. *Robotized Transcranial Magnetic Stimulation*. (Springer Science & Business
756 Media, 2014).
- 757 28. Toschi, N., Welt, T., Guerrisi, M. & Keck, M. E. A reconstruction of the conductive
758 phenomena elicited by transcranial magnetic stimulation in heterogeneous brain tissue.
759 *Phys. Med.* **24**, 80–86 (2008).
- 760 29. Ravazzani, P., Ruohonen, J., Grandori, F. & Tognola, G. Magnetic stimulation of the
761 nervous system: induced electric field in unbounded, semi-infinite, spherical, and cylindrical
762 media. *Ann. Biomed. Eng.* **24**, 606–616 (1996).
- 763 30. Thielscher, A. & Kammer, T. Linking physics with physiology in TMS: a sphere field
764 model to determine the cortical stimulation site in TMS. *Neuroimage* **17**, 1117–1130 (2002).
- 765 31. Fregni, F., Simon, D. K., Wu, A. & Pascual-Leone, A. Non-invasive brain stimulation for

- 766 Parkinson's disease: a systematic review and meta-analysis of the literature. *J. Neurol.*
767 *Neurosurg. Psychiatry* **76**, 1614–1623 (2005).
- 768 32. Hamid, P., Malik, B. H. & Hussain, M. L. Noninvasive Transcranial Magnetic Stimulation
769 (TMS) in Chronic Refractory Pain: A Systematic Review. *Cureus* **11**, e6019 (2019).
- 770 33. Deep Brain Stimulation for the Treatment of Alzheimer Disease and Dementias. *World*
771 *Neurosurg.* **80**, S28.e1-S28.e8 (2013).
- 772 34. Bowary, P. & Greenberg, B. D. Noninvasive Focused Ultrasound for Neuromodulation: A
773 Review. *Psychiatr. Clin. North Am.* **41**, 505–514 (2018).
- 774 35. Lipsman, N. *et al.* MR-guided focused ultrasound thalamotomy for essential tremor: a
775 proof-of-concept study. *Lancet Neurol.* **12**, 462–468 (2013).
- 776 36. Martin, E., Jeanmonod, D., Morel, A., Zadicario, E. & Werner, B. High-intensity focused
777 ultrasound for noninvasive functional neurosurgery. *Ann. Neurol.* **66**, 858–861 (2009).
- 778 37. Resting state functional connectivity changes after MR-guided focused ultrasound mediated
779 blood-brain barrier opening in patients with Alzheimer's disease. *Neuroimage* **200**, 275–280
780 (2019).
- 781 38. Nicodemus, N. E. *et al.* Focused transcranial ultrasound for treatment of neurodegenerative
782 dementia. *Alzheimer's & Dementia: Translational Research & Clinical Interventions* **5**,
783 374–381 (2019).
- 784 39. Jeong, H. *et al.* A pilot clinical study of low-intensity transcranial focused ultrasound in
785 Alzheimer's disease. *Ultrasonography* **40**, 512–519 (2021).
- 786 40. Beisteiner, R. *et al.* Transcranial Pulse Stimulation with Ultrasound in Alzheimer's
787 Disease—A New Navigated Focal Brain Therapy. *Adv. Sci. Lett.* **7**, 1902583 (2020).
- 788 41. Dörl, G., Matt, E. & Beisteiner, R. Functional Specificity of TPS Brain Stimulation Effects

- 789 in Patients with Alzheimer’s Disease: A Follow-up fMRI Analysis. *Neurology and Therapy*
790 **11**, 1391–1398 (2022).
- 791 42. Transcranial ultrasound neuromodulation for epilepsy: A pilot safety trial. *Brain Stimul.* **17**,
792 7–9 (2024).
- 793 43. Lee, C.-C. *et al.* Pilot study of focused ultrasound for drug-resistant epilepsy. *Epilepsia* **63**,
794 162–175 (2022).
- 795 44. Safety of focused ultrasound neuromodulation in humans with temporal lobe epilepsy. *Brain*
796 *Stimul.* **14**, 1022–1031 (2021).
- 797 45. A systematic review of preclinical and clinical transcranial ultrasound neuromodulation and
798 opportunities for functional connectomics. *Brain Stimul.* **17**, 734–751 (2024).
- 799 46. La, T.-G. & Le, L. H. Flexible and Wearable Ultrasound Device for Medical Applications:
800 A Review on Materials, Structural Designs, and Current Challenges. *Advanced Materials*
801 *Technologies* **7**, 2100798 (2022).
- 802 47. Pang, C., Lee, C. & Suh, K.-Y. Recent advances in flexible sensors for wearable and
803 implantable devices. *J. Appl. Polym. Sci.* **130**, 1429–1441 (2013).
- 804 48. Rathod, V. T. A Review of Acoustic Impedance Matching Techniques for Piezoelectric
805 Sensors and Transducers. *Sensors* **20**, 4051 (2020).
- 806 49. Afzal, S. *et al.* Preparation and Evaluation of Polymer-Based Ultrasound Gel and Its
807 Application in Ultrasonography. *Gels* **8**, (2022).
- 808 50. Hu, Y.-Y. *et al.* Transcranial low-intensity ultrasound stimulation for treating central
809 nervous system disorders: A promising therapeutic application. *Front. Neurol.* **14**, 1117188
810 (2023).
- 811 51. Wang, C. *et al.* Bioadhesive ultrasound for long-term continuous imaging of diverse organs.

- 812 *Science* **377**, 517–523 (2022).
- 813 52. Lee, S.-M. *et al.* Calcium-Modified Silk Patch as a Next-Generation Ultrasound Coupling
814 Medium. *ACS Appl. Mater. Interfaces* **13**, 55827–55839 (2021).
- 815 53. Molerón, M., Serra-Garcia, M. & Daraio, C. Acoustic Fresnel lenses with extraordinary
816 transmission. *Appl. Phys. Lett.* **105**, 114109 (2014).
- 817 54. White, P. J., Clement, G. T. & Hynynen, K. Local frequency dependence in transcranial
818 ultrasound transmission. *Phys. Med. Biol.* **51**, 2293–2305 (2006).
- 819 55. Hayner, M. & Hynynen, K. Numerical analysis of ultrasonic transmission and absorption of
820 oblique plane waves through the human skull. *J. Acoust. Soc. Am.* **110**, 3319–3330 (2001).
- 821 56. Legon, W. *et al.* Transcranial focused ultrasound modulates the activity of primary
822 somatosensory cortex in humans. *Nat. Neurosci.* **17**, 322–329 (2014).
- 823 57. Gâteau, J. *et al.* Transcranial ultrasonic therapy based on time reversal of acoustically
824 induced cavitation bubble signature. *IEEE Trans. Biomed. Eng.* **57**, 134–144 (2010).
- 825 58. Lee, W., Weisholtz, D. S., Strangman, G. E. & Yoo, S.-S. Safety Review and Perspectives
826 of Transcranial Focused Ultrasound Brain Stimulation. *Brain Neurorehabil* **14**, e4 (2021).
- 827 59. Luo, H. *et al.* Forward osmosis with electro-responsive P(AMPS-co-AM) hydrogels as draw
828 agents for desalination. *J. Memb. Sci.* **593**, 117406 (2020).
- 829 60. Hsieh, J.-C. *et al.* Design of an injectable, self-adhesive, and highly stable hydrogel
830 electrode for sleep recording. *Device* **0**, (2023).
- 831 61. Hsieh, J.-C. *et al.* A highly stable electrode with low electrode-skin impedance for wearable
832 brain-computer interface. *Biosens. Bioelectron.* **218**, 114756 (2022).
- 833 62. Lee, C.-J. *et al.* Ionic Conductivity of Polyelectrolyte Hydrogels. *ACS Appl. Mater.*
834 *Interfaces* **10**, 5845–5852 (2018).

- 835 63. Ashkani, M., Bouhendi, H., Kabiri, K. & Rostami, M. R. Synthesis of poly (2-acrylamido-2-
836 methyl propane sulfonic acid) with high water absorbency and absorption under load (AUL)
837 as concrete grade superabsorbent and its performance. *Construction and Building Materials*
838 **206**, 540–551 (2019).
- 839 64. Sekizkardes, B., Su, E. & Okay, O. Mechanically Strong Superabsorbent Terpolymer
840 Hydrogels Based on AMPS via Hydrogen-Bonding Interactions. *ACS Applied Polymer*
841 *Materials* (2023) doi:10.1021/acsapm.2c02085.
- 842 65. Chen, H. J. *et al.* Moisture retention of glycerin solutions with various concentrations: a
843 comparative study. *Sci. Rep.* **12**, 10232 (2022).
- 844 66. Shen, G. *et al.* A novel flexible hydrogel electrode with a strong moisturizing ability for
845 long-term EEG recording. *J. Neural Eng.* **18**, (2021).
- 846 67. Zhang, K. *et al.* Metagel with Broadband Tunable Acoustic Properties Over Air–Water–
847 Solid Ranges. *Adv. Funct. Mater.* **29**, 1903699 (2019).
- 848 68. Laugier, P. & Haïat, G. Introduction to the Physics of Ultrasound. *Bone Quantitative*
849 *Ultrasound* 29–45 (2011).
- 850 69. Nguyen, J. L., Schwartz, J. & Dockery, D. W. The relationship between indoor and outdoor
851 temperature, apparent temperature, relative humidity, and absolute humidity. *Indoor Air* **24**,
852 103–112 (2014).
- 853 70. Human responses to high humidity in elevated temperatures for people in hot-humid
854 climates. *Build. Environ.* **114**, 257–266 (2017).
- 855 71. Leigh, B. L. *et al.* Antifouling Photograftable Zwitterionic Coatings on PDMS Substrates.
856 *Langmuir* **35**, 1100–1110 (2019).
- 857 72. Kim, D.-H. *et al.* Epidermal electronics. *Science* **333**, 838–843 (2011).

- 858 73. Rossetti, A. O. & Laureys, S. *Clinical Neurophysiology in Disorders of Consciousness:*
859 *Brain Function Monitoring in the ICU and Beyond.* (Springer, 2015).
- 860 74. Allison, T. *et al.* Human cortical potentials evoked by stimulation of the median nerve. II.
861 Cytoarchitectonic areas generating short-latency activity. *J. Neurophysiol.* (1989)
862 doi:10.1152/jn.1989.62.3.694.
- 863 75. Buzsáki, G. & Draguhn, A. Neuronal oscillations in cortical networks. *Science* **304**, 1926–
864 1929 (2004).
- 865 76. Makeig, S., Debener, S., Onton, J. & Delorme, A. Mining event-related brain dynamics.
866 *Trends Cogn. Sci.* **8**, 204–210 (2004).
- 867 77. Yamada, T., Kimura, J., Wilkinson, J. T. & Kayamori, R. Short- and long-latency median
868 somatosensory evoked potentials. Findings in patients with localized neurological lesions.
869 *Arch. Neurol.* **40**, 215–220 (1983).
- 870 78. Poornima, S., Ali, S. S., Balaji, P. A., Shankar, V. & Kutty, K. Median nerve somatosensory
871 evoked potentials in medical students: Normative data. *Adv. Biomed. Res.* **2**, 56 (2013).
- 872 79. Hlushchuk, Y. & Hari, R. Transient suppression of ipsilateral primary somatosensory cortex
873 during tactile finger stimulation. *J. Neurosci.* **26**, 5819–5824 (2006).
- 874 80. Tang, Y. & Kim, E. S. *Simple Sacri Fi Cial-Layer-Free Microfabrication Processes for Air-*
875 *Cavity Fresnel Acoustic Lenses (ACFALs) with Improved Focusing Performance.* (2022).
- 876 81. Bhattacharya, S., Datta, A., Berg, J. M. & Gangopadhyay, S. Studies on surface wettability
877 of poly(dimethyl) siloxane (PDMS) and glass under oxygen-plasma treatment and
878 correlation with bond strength. *J. Microelectromech. Syst.* **14**, 590–597 (2005).
- 879 82. Lee, B. W., Ryeom, J., Ko, Y. H., Kim, K. J. & Ko, J.-H. Acoustic anisotropy of oriented
880 polyethylene terephthalate films studied through Brillouin light scattering. *J. Soc. Inf. Disp.*

881 **15**, 201–205 (2014).

882 83. Auditory event-related dynamics of the EEG spectrum and effects of exposure to tones.

883 *Electroencephalogr. Clin. Neurophysiol.* **86**, 283–293 (1993).

884